Journal of Solid State Chemistry 181 (2008) 2646–2652

Contents lists available at ScienceDirect

Journal of Solid State Chemistry

journal homepage: www.elsevier.com/locate/jssc

A series of aluminum tungsten oxides crystallizing in a new ReO_3-related structure type

Frank Krumeich *, Greta R. Patzke [1]

Laboratory of Inorganic Chemistry, ETH Zurich, CH-8093 Zurich, Switzerland

ARTICLE INFO

Article history:
Received 17 April 2008
Received in revised form
26 May 2008
Accepted 7 June 2008
Available online 12 June 2008

Keywords:
Aluminum tungsten oxide
Shear structure
Electron diffraction
HRTEM
Z contrast

ABSTRACT

A series of new aluminum tungsten oxides with the general formula $Al_4W_{2n}O_{6n+2}$ ($n = 4$–7) was found and structurally characterized by electron diffraction, high-resolution transmission electron microscopy (HRTEM) and high angle annular dark field scanning transmission electron microscopy (HAADF-STEM). The structural model for $Al_4W_{10}O_{32}$ (*I*4/*mmm* (space group no. 139); $a \approx 0.375$, $c \approx 3.95$ nm) consists of slabs of $[5 \times \infty \times \infty]$ corner-sharing WO_6 octahedra that are connected via edge-sharing to AlO_6 octahedra. Simulated HRTEM images agree well with the experimental ones and thus support the proposed structural model. The connection between adjacent slabs of WO_3 via AlO_6 octahedra represents a novel variant of crystallographic shear operation for ReO_3-type structures. The crystallites display a wide range of stacking sequences that are frequently intergrown with each other.

1. Introduction

In the pseudobinary system Al_2O_3/WO_3, only one stable phase, namely $Al_2(WO_4)_3$ ($\equiv Al_2W_3O_{12}$), has been characterized up to now [1]. Its orthorhombic structure comprises a three-dimensional network of WO_4 tetrahedra and AlO_6 octahedra connected via corner-sharing with each other. Furthermore, a W-rich phase ($Al_2W_{24}O_{74}$) forms at 400 °C and is stable till 830 °C [2]. It is described as a cubic isotype of ReO_3 ($a = 0.378$ nm) with both metals located in an octahedral oxygen coordination. Such octahedra also appear in the aluminum tungstate(V) $AlWO_4$, which forms a rutile-like structure [3]. Recent investigations uncovered a series of Al–W oxides that crystallize in a novel structure type related to ReO_3 [4].

The cubic ReO_3 structure consists of Re-centered oxygen octahedra (ReO_6) connected by corner-sharing in such a way that their centers are arranged on a primitive cubic lattice [5]. The ReO_3 type represents the prototype for many structures with the general composition MX_3. Moreover, it is the basis of very versatile structural concepts, for example, block structures, tungsten bronzes and perovskites [6–9]. Different polymorphs of WO_3 crystallize in distorted variants of the ReO_3 type, as firstly shown by Bräkken already in 1931 [10]. Many structures are derived from this type by the so-called crystallographic shear operation [11,12]: planes of oxygen atoms are formally removed in such a way that the ReO_3-type parent structure is cut into well-defined slabs or blocks. Subsequently, planes of edge-sharing octahedra are introduced between ReO_3-type areas by reconnecting the octahedra. As the overall effect, the oxygen–metal ratio is decreased like for example in the reduced tungsten oxides (Magnéli phases W_nO_{3n-1}). Here, parallel shear planes occur between $[n \times \infty \times \infty]$ arrays of corner-sharing octahedra [13–15]. Furthermore, also ternary and quaternary tungsten oxides exist that form structures comprising cuttings of the ReO_3 type. In the Nb-rich part of the system Nb_2O_5/WO_3, such shear planes appear in two perpendicular directions so that $[n \times m \times \infty]$ blocks of the ReO_3-type structure arise [16,17]. A structural alternative to forming planes with edge-sharing octahedra is the incorporation of planes of other structural elements into the gap between ReO_3-type slabs. Examples are units of the tetragonal tungsten bronze type that are built in between WO_3 areas in $W_{12}O_{34}$ [18] and in W-rich niobium tungsten oxides [19,20]. Moreover, alternating slabs of a tungsten bronze with hexagonal tunnels and of WO_3 exist in the intergrowth tungsten bronzes [21,22].

HRTEM images of the new Al–W oxides show that these structures comprise ReO_3-type slabs as well but the connection between them does not correspond to any of the connection types already known. The derivation of a structure model as well as the characterization of polytypes and of stacking disorder by electron microscopy are presented in the following.

2. Experimental

2.1. Synthesis

The decomposition of $(NH_4)_{0.26}WO_3$ and the subsequent reaction of gaseous WO_3 with an alumina crucible at 1500 °C

* Corresponding author. Fax: +41 446321149.
E-mail address: krumeich@inorg.chem.ethz.ch (F. Krumeich).
[1] Present address: Institute of Inorganic Chemistry, University of Zurich, CH-8057 Zurich, Switzerland.

0022-4596/$ - see front matter © 2008 Elsevier Inc. All rights reserved.
doi:10.1016/j.jssc.2008.06.013

lead to a mixture of different phases according to the results of X-ray powder diffraction (Fig. 1a).

2.2. Electron microscopy

Transmission electron microscopy (TEM) was performed on a *CM30* microscope (*FEI*, Eindhoven; *SuperTwin* lens with $C_s = 1.2$ mm; LaB_6 cathode, operated at 300 kV). The material was crushed in an agate mortar and dispersed in ethanol. Some drops were deposited on a perforated carbon foil supported by a copper grid. Thin crystal fragments were selected in the diffraction mode of the microscope and oriented along zone axes with low indices using a double tilt holder. Selected area electron diffraction (SAED) patterns and high-resolution transmission electron microscopy (HRTEM) images were recorded on either on a CCD camera or on photographic plates. In the latter case, prints were made from the negatives and subsequently scanned for further electronic processing. Simulations of HRTEM images were calculated using the multi-slice algorithm and of electron diffraction patterns by a kinematical approximation (*EMS* package [23]). The simulations of the HRTEM images in Fig. 4c were obtained with the following microscope parameters: defocus $f = -40$ nm, spherical aberration $C_s = 1.2$ mm, chromatic aberration $C_c = 2$ mm, focus spread $\Delta f = 10$ nm, reciprocal radius of the objective aperture $R^{-1} = 9.0\,\mathrm{nm}^{-1}$, beam convergence = 1.0 mrad.

Scanning transmission electron microscopy (STEM) was performed on a field emission electron microscope (*Tecnai 30F*, *FEI*, Eindhoven; *SuperTwin* lens), operated at 300 kV (gun extraction voltage: 4.25 kV). STEM images were recorded with a high angle annular dark field (HAADF) detector (image size: 1024×1024 pixels; scan times: ca. 15 s; camera length: 200 mm). The use of mainly incoherently scattered electrons for image formation results in atomic number contrast (*Z* contrast) [24]. The images were smoothed to reduce noise and scanning artifacts [25].

Energy-dispersive X-ray (EDX) spectrometers attached to both microscopes allowed us to perform elemental analyses of the investigated crystallites. For image processing, the software *Digital Micrograph* (*Gatan*) was used.

3. Results and discussion

The X-ray powder diffractogram (XRD) of the product (Fig. 1a) shows a number of well-defined, sharp peaks with high intensity and broad ones with much lower intensity. Obviously, the product contains a phase mixture which prevents an unambiguous assignment of the phases. The strong reflections indicate that WO_3 is the main constituent, with the data best fitting to a cubic modification ($a = 0.752$ nm [26]). The additional broad reflections that have a low intensity cannot be assigned to any known tungsten oxide derivative. EDX analyses of different crystal fragments in the transmission electron microscope show that an aluminum tungsten oxide is formed along with pure WO_3 (Fig. 1b). Indeed, comprehensive TEM studies of the reaction product revealed that a minor part of the reaction product represents a hitherto unknown phase. It should be noted that during the TEM investigations electron diffraction patterns (not shown here) were obtained that correspond to different WO_3 polymorphs.

3.1. Electron diffraction

The reciprocal space of selected crystallites was explored by SAED investigations. Typical SAED patterns of the new phases (Fig. 2) show a short repeat distance of the reflections in one direction pointing to a long axis and, perpendicular to that, a relatively large distance corresponding to ~0.375 nm in real space. There is a significant variation of the reflection intensity along the long axis and the brightest spots indicate the presence of a substructure with a length of ~0.38 nm. Between the substructure reflections, the varying spot distance indicates the occurrence of different ordering variants: some of the crystallites investigated show four distinct superstructure reflections (Fig. 2a), others three (Fig. 2b) or six of them (Fig. 2c). In the SAED patterns of many crystallites, however, there is only diffuse streaking between the sharp and strong reflections of the substructure (Fig. 2d), indicating the presence of disorder. The short crystallographic axis (~0.375 nm) and the distance between the substructure reflections along the long axis (~0.38 nm) approximately correspond to

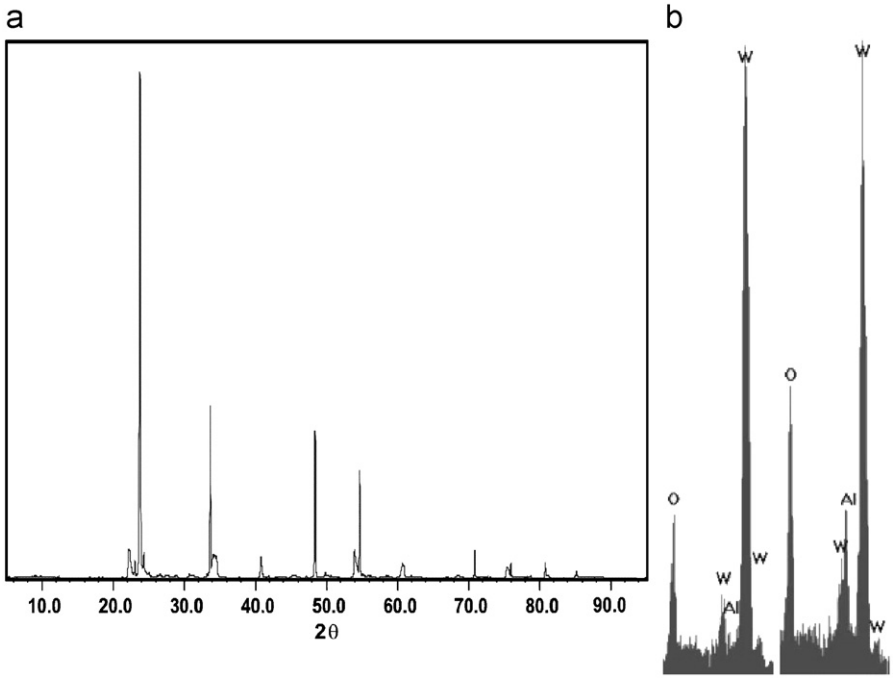

Fig. 1. (a) X-ray powder diffractogram (XRD) of the product. (b) Sections of the EDX spectra of crystallites of WO_3 (left) and of the new phase containing Al (right).

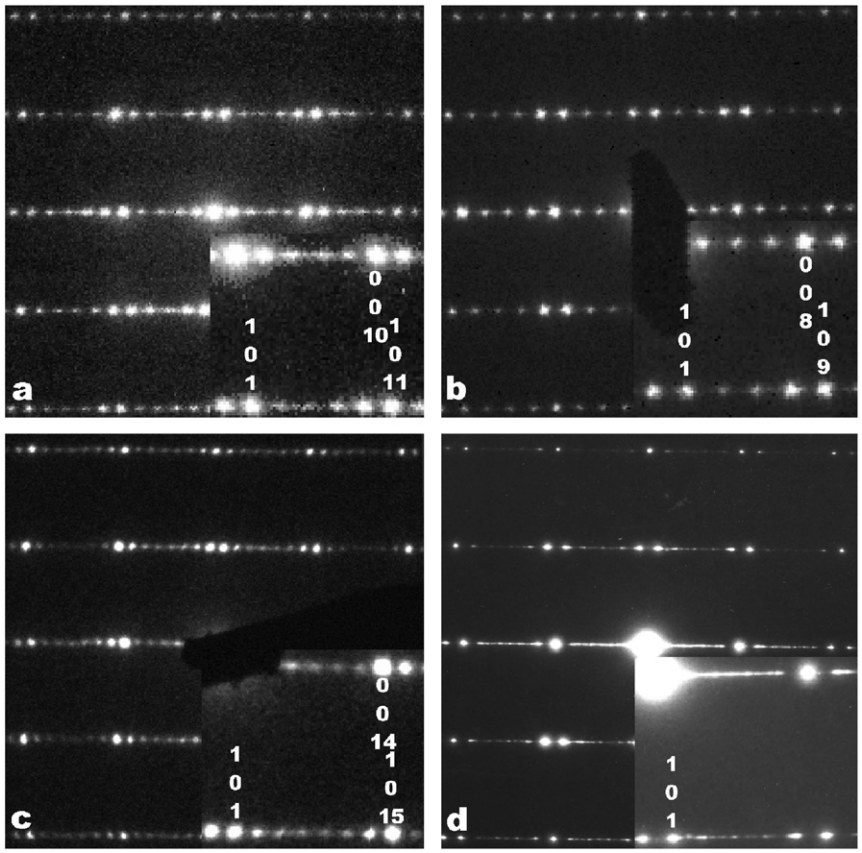

Fig. 2. Selected area electron diffraction (SAED) patterns of differently ordered crystallites observed along [010]. The insets on the lower right side of each show a magnified section with the origin of reciprocal space being in the top left corner and with indices assigned to some reflections: (a) four superstructure reflections, $c \approx 3.95$ nm; (b) three superstructure reflections, $c \approx 3.2$ nm; (c) six superstructure reflections, $c \approx 5.53$ nm; and (d) heavily disordered crystal. The superstructure reflections have vanished completely and diffuse scattering present along the c^*-axis indicates stacking disorder.

the diagonal of a WO_6 octahedron. For comparison, W–O distances between 0.173 and 0.220 nm appear in tetragonal WO_3 [27]. Since the distances of ~0.38 nm occur along perpendicular directions, they indicate the presence of a structure related to the ReO_3 type.

It should be noted that the presence of Al in the investigated crystallites was confirmed by EDX spectroscopy (Fig. 1b). An approximate quantification points to large variations of the ratio Al:W of different crystallites (Al:W ≈ 1:4–1:2). This detection of large compositional fluctuations is certainly significant. However, the quantification of the EDX spectra was performed with the approximate Cliff–Lorimar factors provided by the acquisition software, so that these results are rather inaccurate and will thus not be discussed further.

For achieving more information about symmetry and metric of the new phase, tilting experiments were performed. Three SAED patterns with low indexed zone axes were obtained by tilting a crystal around the long axis (Fig. 3a–c). The reconstruction of the reciprocal lattice from these data indicates that the length of the axis in the third direction is equal to that of the short axis. Furthermore, the angles between the three zone axes as measured approximately with the goniometer of the microscope agree quite well with those for a tetragonal unit cell: measured angles $[100]/[2\bar{1}0] = 24^\circ$ (theoretical value $= 26.56^\circ$); $[2\bar{1}0]/[1\bar{1}0] = 20^\circ$ (18.44°). It is evident from these results that the new phases most likely crystallize with tetragonal symmetry. As an example, the lattice parameters are $a \approx 0.375$ and $c \approx 3.95$ nm for the 10-fold superstructure.

In the SAED patterns recorded along [010] (Fig. 2), the reflections with odd values for $h+l$ are systematically absent. The observed reflection condition $h+l = 2n$ for $h\,0\,l$ arises from a centered cell. All these findings are in perfect agreement with a body-centered tetragonal unit cell. The observed restrictions are fulfilled by the space group $I4/mmm$, being that with the highest symmetry possible for the reflection condition observed here. In the following, it is used for the structure description although all body-centered tetragonal space groups would give rise to similar diffraction patterns for the zone axes observed experimentally here. The positions of the reflections in kinematical simulations (insets in Fig. 3) calculated with the structure parameters listed in Table 1 agree with those in the observed SAED patterns.

SAED patterns recorded along the c-axis support this interpretation: the most intense reflections correspond to those in the simulations (Fig. 3d). However, additional weak spots appear that violate the reflection condition $h+k = 2n$. Furthermore, almost circular diffuse scattering is present around these weak spots. EDXS analyses of crystals showing this type of SAED patterns prove the presence of Al, and it thus is most likely that they belong to the new phases. The observation of additional reflections and diffuse scattering in the SAED patterns along [001] is apparently caused by the stacking faults in direction of the c-axis (cf. Fig. 2d) but a comprehensive explanation has not been achieved yet.

3.2. Derivation of the structural model

HRTEM images recorded along the b-axis reveal the main characteristics of the new structure as well as information about defects (Fig. 4). It is evident that the structure is layered

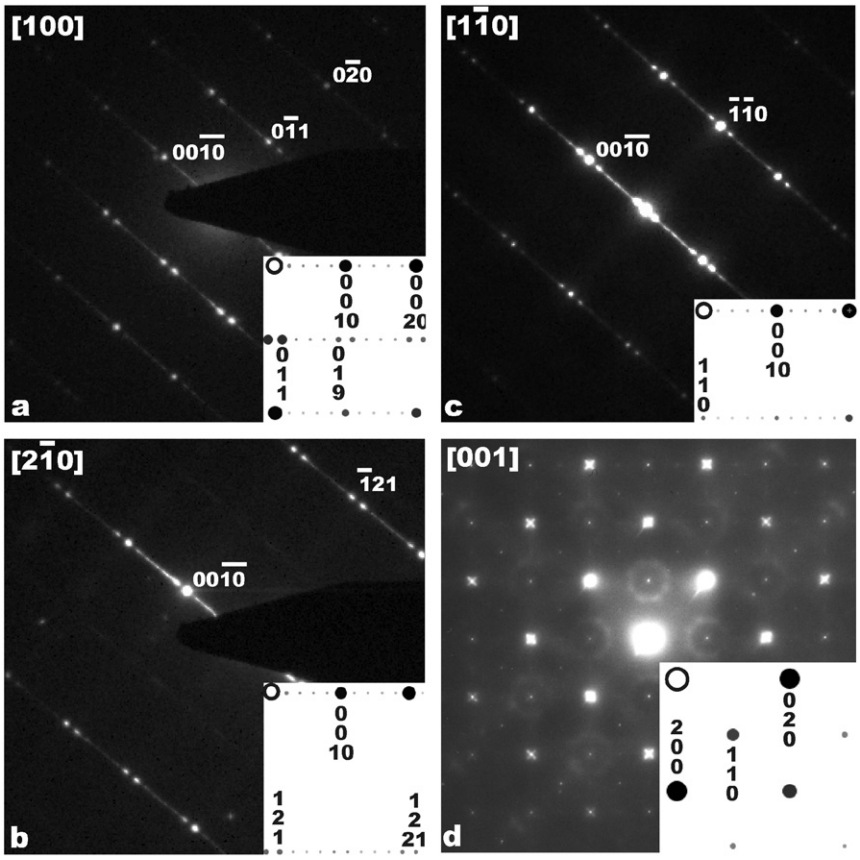

Fig. 3. SAED patterns: (a–c) tilt series around the c^*-axis and (d) along [010]. Zone axes and indices of some reflections are given. The insets on the lower right side show sections of kinematical simulations calculated with the structural data from Table 1. The origin of reciprocal space (top left corner) is marked by an open circle.

Table 1
Atomic coordinates for the structural model of $Al_4W_{10}O_{32}$ derived from electron microscopy results (space group: $I4/mmm$ (no. 139); $a \approx 0.375$, $c \approx 3.95$ nm)

Atom	Multiplicity Wyckoff letter	x	y	z
Al	4*d*	0.5	0	0.25
W_1	2*a*	0	0	0
W_2	4*e*	0	0	0.1
W_3	4*e*	0	0	0.2
O_1	4*e*	0	0	0.05
O_2	4*e*	0	0	0.15
O_3	4*e*	0	0	0.25
O_4	4*c*	0	0.5	0
O_5	8*g*	0	0.5	0.1
O_6	8*g*	0	0.5	0.2

comprising slabs of different width that appear as square arrays of black and white patches. These slabs are quasi-indefinitely running along the *a*-axis but are separated by lines of dark contrast in direction of the *c*-axis (Fig. 4a). In well-ordered regions with the 10-fold superstructure (Fig 4b and c), there are slabs of $[5 \times \infty]$ black dots. In projection along the *b*-axis, these slabs are shifted by $1/2a+1/2c$ with respect to each other. This shift is in accordance with the body-centered tetragonal cell derived from the results of electron diffraction investigations. Although the 10-fold structure is perfect here in quite large areas, stacking faults appear with deviating slab width (Fig. 4a). Since all HRTEM images shown here were recorded close to Scherzer defocus, the black patches apparently represent the projection of those columns that contain the highest scattering potential in this system and therefore correspond to the positions of the W-centered octahedra.

This interpretation of the HRTEM image contrast is confirmed by the results of the HAADF-STEM (*Z* contrast) investigations (Fig. 5). The images show the projection of the W positions unambiguously as bright dots since W has by far the highest atomic number of the elements constituting the given phase. A direct comparison for the 10-fold superstructure (Fig. 5a) demonstrates that the bright dots in the *Z* contrast image are indeed located on exactly the same sites as the dark dots in the HRTEM images.

In the highly resolved images of the structure obtained by both methods (Fig. 5a), the distance between the dots of the square arrangement within the slabs is ca. 0.38 nm. This value approximately corresponds to the length of the diagonal in a WO_6 octahedron. This observation in conjunction with the information obtained from electron diffraction indicates that the structure inside the slabs is basically that of ReO_3-type WO_3.

On the first view, the contrast of the HRTEM images (Fig. 4) look somewhat similar to those observed for tungsten oxides with crystallographic shear planes: there are parallel slabs with a square dot pattern that are separated by lines. In the intermediate space between the square dot arrays in the slabs, no characteristic contrast features can be distinguished in the images here. In the HRTEM images, the contrast there is gray in thin and almost black in thick areas (top and bottom parts, respectively, in Fig. 4b and c). In the HAADF-STEM images (Fig. 5), the contrast between the slabs is always dark, which means that the scattering potential located there is much lower than that of the W-containing columns, which are visible as bright patches. From this contrast and the measured distance between the slabs, it must be

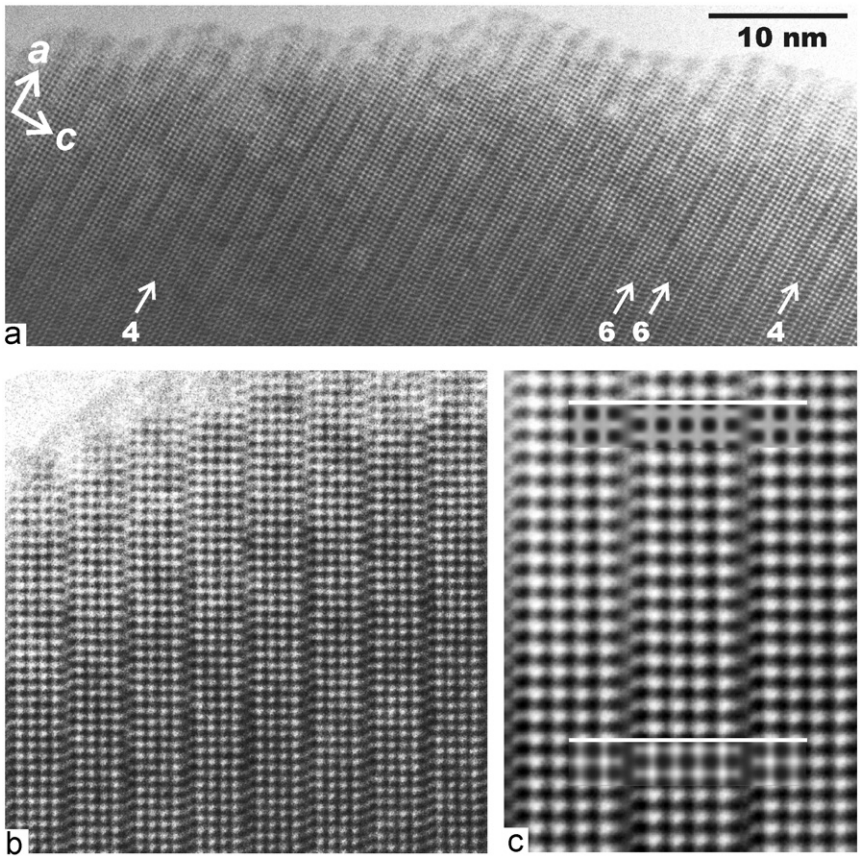

Fig. 4. (a) HRTEM image along [010]. Most areas show the 10-fold superstructure (5W atoms per slab) but some slabs with four and six rows of WO_6 octahedra are present as well (arrows). (b) Magnified area with the perfect 10-fold superstructure. (c) Enlargement of (b) (Fourier filtered). Simulations calculated with the structural data of $Al_4W_{10}O_{32}$ (Table 1) for thicknesses of 1.5 nm (top) and of 4.5 nm (bottom) are shown as insets and marked by white lines (length = 3.95 nm) above them for better visibility.

concluded that a new type of connection between the *Re*O_3-type slabs appears here that does not correspond to any of the structures described up to now (see Introduction).

To construct a structural model for the 10-fold superstructure, only the information that is unambiguously extractable from the evaluation of the electron microscopy results was used. The WO_6 octahedra were placed onto the positions of the dark patches in the HRTEM that correspond to the bright patches in the *Z* contrast images (Fig. 5a). Because of the high symmetry of the selected space group *I*4/*mmm*, W occupies three independent sites only (Table 1). The O atoms were placed in the middle between adjacent W positions resulting in ideal WO_6 octahedra. Adjacent slabs of $[5 \times \infty \times \infty]$ WO_6 octahedra (gray in Fig. 6) are shifted by $[\frac{111}{222}]$ in respect of each other. This arrangement of the *Re*O_3-type slabs creates empty octahedral sites at the boundary between neighboring slabs. Filling these sites by Al leads to the structural model represented in Fig. 6. The AlO_6 octahedra are attached to the WO_3 slabs by sharing edges. Thereby, chains of corner-sharing AlO_6 octahedra are formed along the *a*- and *b*-axes. Two adjacent chains of AlO_6 octahedra with a relative displacement of $[\frac{11}{22}0]$ are connected by edge-sharing. Each AlO_6 octahedron shares four edges with other AlO_6 octahedra and the other four edges with adjacent WO_6 octahedra. As a result, a plane of AlO_6 octahedra arises that connects the WO_3 slabs.

The correctness of the structural model was probed by simulating HRTEM images using the parameters of the model (Table 1) and of the TEM microscope (see Experimental). The calculated images are in good agreement with the experimental one (Fig. 4c). The image contrast is of course dominated by the high scattering potential of the W atoms but the Al positions contribute to the gray contrast between the WO_3 slabs; faintly in thin areas (Fig. 4c top) and more strongly in thicker areas (Fig. 4c bottom). If simulations were calculated with a structural model containing no Al atoms for comparison, they show a uniformly gray contrast there which is thickness independent.

It cannot be excluded that the symmetry of the body-centered cell is reduced compared to this model in space group *I*4/*mmm*, e.g. by tilt or distortion of octahedra. However, all experimental results at hand can satisfactorily be explained by the model presented here so that the deviation of the actual structure from this possibly idealized model is expected to be small.

Edge-sharing of AlO_6 octahedra, for example, occurs also in the structure of corundum (besides face-sharing). As for WO_6 octahedra, edge-sharing has been observed in reduced phases of the WO_{3-x} type (Magnéli phases). The observed types of coordination for Al and W are thus not unusual in their own right, but the resulting interface structure connecting the *Re*O_3-type slabs is without precedence as far as we know. Formally, the first step in generating the structure of $Al_4W_{10}O_{32}$ is to cut the WO_3 structure into slabs of $[5 \times \infty \times \infty]$ octahedra like in the crystallographic shear operation [11,12]. In contrast to that, no oxygen atoms are removed and no direct connection between the slabs by edge-sharing is formed here. Instead, a plane of AlO_6 octahedra is fit in between the *Re*O_3-type slabs. However, here the connection occurs via edge-sharing of the octahedra as well. Thus, this novel structure might also be regarded as a variant of crystallographic shear in *Re*O_3-type compounds. The $Al_4W_{10}O_{32}$ structure appears to be very flexible and can accommodate

varying Al:W ratios since rows of WO_6 octahedra can easily be added or removed leading to polytypes (see below) and stacking faults (Fig. 4a).

The stoichiometry of the structural model for the 10-fold superstructure is $Al_4W_{10}O_{32}$ (Table 1). Interestingly, this composition corresponds to a not fully oxidized phase. If W^{6+} would exclusively be present, the composition should be $Al_4W_{10}O_{36}$ instead of $Al_4W_{10}O_{32}$ as found for the structural model. This deviation might indeed be caused by the occurrence of reduced W but additional Al on W sites or not fully occupied Al positions are more reasonable explanations. Such a less-ordered occupancy of different metal positions might also lead to the deviation from ideal symmetry that has been detected by electron diffraction along [001] (Fig 3d). In addition, the observation of circular diffuse scattering indicates the presence of short-range order in the cation sublattice.

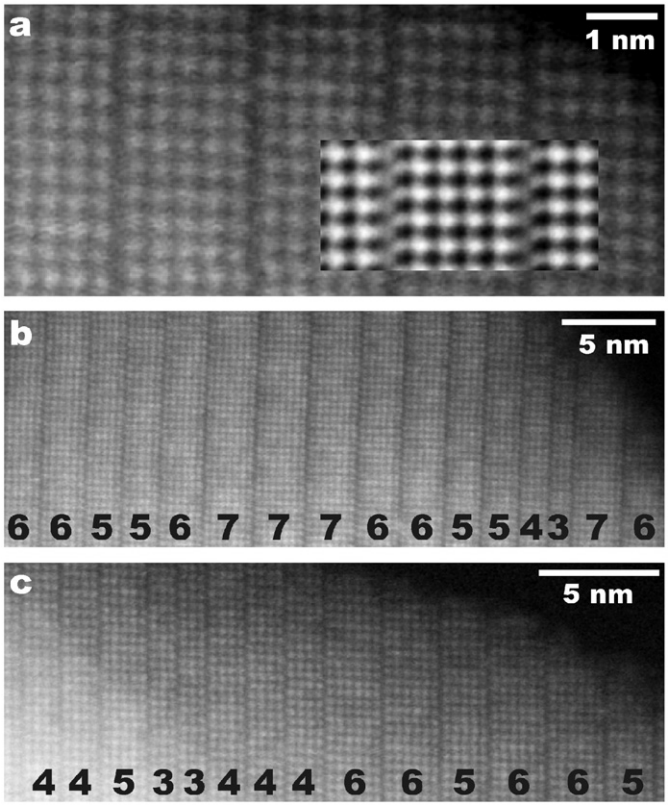

Fig. 5. HAADF-STEM images along [010] (smoothed) show the W positions as bright patches that are located in slabs separated by dark lines. (a) Highly magnified area of $Al_4W_{10}O_{32}$ with 5W atoms wide slabs. For comparison, a section of the HRTEM image (cutting of Fig. 4c) is shown as inset. The bight patches in the HAADF-STEM and the dark ones in the HRTEM image appear at the same positions. (b, c) Disordered areas with varying widths of the WO_3 slabs. The width of each slab is given by number of W atoms.

3.3. Polytypes and disorder

The SAED patterns of the a^*c^* plane prove that different polytypes of the novel aluminum tungsten oxide exist (Fig. 1a–c). Four superstructure reflections indicate a 10-fold ($c \approx 3.95$ nm), three superstructure reflections an eight-fold ($c \approx 3.2$ nm) and six superstructure reflections a 14-fold superstructure ($c \approx 5.53$ nm), respectively. However, additional diffuse streaking which appears along c^* in all SAED patterns points to the omnipresence of stacking disorder. In heavily disordered crystals, the superstructure reflections have vanished completely and exclusively the substructure reflections are still observed (Fig. 1d).

The characteristic of $Al_4W_{10}O_{32}$ with the 10-fold superstructure are slabs of 5W atoms in width. As discussed above, these slabs are directly visible in HRTEM (Fig. 4) as well as in HAADF-STEM images (Fig. 5a). The polytypes are derived from this structure by adding or removing planes of WO_6 octahedra. Because this has to be done in both slabs present in a unit cell, two units of WO_3 have to be added or subtracted to calculate the composition of a certain polytype. Consequently, the general formula for this series of alumina tungsten oxides is $Al_4W_{2n}O_{6n+2}$. By electron diffraction, the existence of the phases with $n = 4$, 5 and 7 has been confirmed in μm-sized regions (Fig. 1a–c). Domains of the missing member with $n = 6$ are often found in the HRTEM and HAADF-STEM images (Figs. 5 and 7). Other members are present in small microdomains, often comprising one or two slabs only. The smallest slab discovered up to now is three W atoms wide ($n = 3$ in Fig. 5c). Interestingly, slabs consisting of more than seven W atoms were only found in a sole crystal fragment yet with the largest slab width being nine W atoms ($n = 9$ in Fig. 7b). In the center of this area, slabs with 7–9W atoms are intergrown while on both sides the members with 4–6 are predominant.

Because of the close structural relationship between these polytypes, intergrowth of them is frequently observed. The crystal region shown in Fig. 7a represents an example for this. Besides the predominant 12-fold superstructure, as recognizable by slabs 6W atoms wide, small domains of the 10-fold superstructure are present as well.

As already indicated by the streaking present in the SAED patterns (Fig. 1), stacking disorder appears frequently. The 10-fold superstructure present in the HRTEM image reproduced in Fig. 4a is well-ordered in most regions but a few slabs are incorporated with one row of black spots (i.e. one plane of WO_6 octahedra) missing (4W per slab) or with one additional row (6W per slab). In fact, many crystallites are more heavily disordered and show a random arrangement of slabs with different width (Figs. 5b, c and 7b). It is obviously typical for this structure type that a perfect constitution of the different phases is

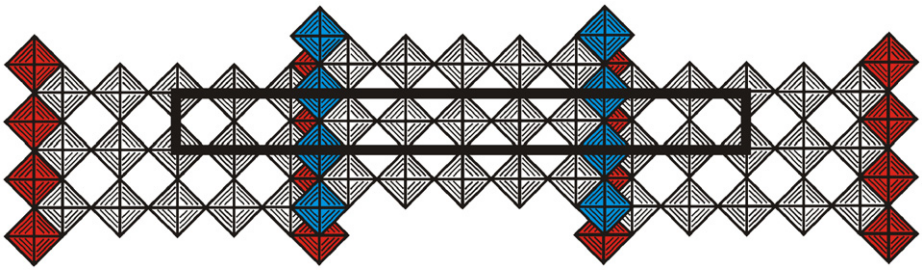

Fig. 6. Structural model for $Al_4W_{10}O_{32}$ in projection along [010]. The unit cell is outlined with the long side corresponding to the crystallographic c-axis. WO_6 octahedra are gray while AlO_6 octahedra are shaded red and blue, respectively.

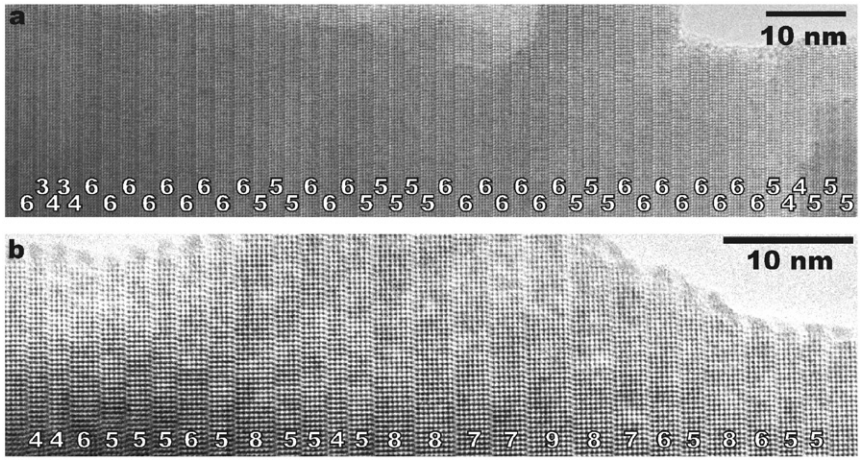

Fig. 7. HRTEM images along [010]: (a) intergrowth of mainly the 10-fold and the 12-fold superstructure and (b) disordered area with varying slab sizes. The width of each slab is given by the number of W atoms.

restricted to small areas only. This statement is supported by all HRTEM and HAADF-STEM images observed till now (see examples in Figs. 4a, 5 and 7).

It should be noted that it was not possible to synthesize one of the phases $Al_4W_{2n}O_{6n+2}$ in pure form up to now. Considering the close structural relationship of these phases as well as their tendency to form intimate intergrowths and stacking variants, the exclusive synthesis of a pure phase appears to be an insurmountable synthetic challenge.

Acknowledgments

We are indebted to Prof. Dr. R. Nesper for the generous support of this work and to Dr. M. Wörle for valuable discussions. We thank the EMEZ (electron microscopy ETH Zurich) for TEM measuring time.

References

[1] D.C. Craig, N.C. Stephenson, Acta Crystallogr. B 24 (1968) 1250–1255.
[2] H.-J. Lunk, M. Salmen, H. Weiner, C. Baeker, W. Wilde, D. Müller, Z. Anorg. Allg. Chem. 568 (1989) 171–177.
[3] J.P. Doumerc, M. Vlasse, M. Pouchard, P. Hagenmuller, J. Solid State Chem. 14 (1974) 144–151.
[4] F. Krumeich, G.R. Patzke, Microsc. Microanal. 13 (Suppl. 3) (2007) 366–367.
[5] K. Meisel, Z. Anorg. Allg. Chem. 207 (1932) 121–128.
[6] B.G. Hyde, M. O'Keefe, Acta Crystallogr. A 29 (1973) 243–248.
[7] B.-O. Marinder, Angew. Chem. Int. Ed. 25 (1986) 431–442.
[8] M.T. Anderson, J.T. Vaughey, K.R. Poeppelmeier, Chem. Mater. 5 (1993) 151–165.
[9] B.G. Hyde, S. Anderson, Inorganic Crystal Structures, Wiley, New York, 1989.
[10] H. Bräkken, Z. Krist. 78 (1931) 484–489.
[11] J.S. Anderson, B.G. Hyde, J. Phys. Chem. Solids 28 (1967) 1393–1408.
[12] J.S. Anderson, J. Phys. Colloq. 38 (C7) (1977) 17–27.
[13] S. Iijima, J. Solid State Chem. 14 (1975) 52–65.
[14] W. Sahle, M. Sundberg, Chem. Scr. 22 (1983) 248–253.
[15] A. Magnéli, Chem. Scr. 26 (1986) 535–546.
[16] R.S. Roth, A.D. Wadsley, Acta Crystallogr. 19 (1965) 42–47.
[17] G. Heurung, R. Gruehn, J. Less-Common Met. 76 (1980) 17–32.
[18] M. Sundberg, Chem. Scr. 14 (1978–1979) 161–166.
[19] P.J. England, J. Booth, R.J.D. Tilley, T. Ekström, J. Solid State Chem. 44 (1982) 60–74.
[20] P.J. England, R.J.D. Tilley, Chem. Scr. 20 (1982) 102–107.
[21] A. Hussain, L. Kihlborg, Acta Crystallogr. A 32 (1976) 551–557.
[22] L. Kihlborg, M. Sundberg, Acta Crystallogr. B 53 (1997) 95–101.
[23] P. Stadelmann, Ultramicroscopy 21 (1987) 131–146.
[24] S.J. Pennycook, Ultramicroscopy 30 (1989) 58–69.
[25] F. Krumeich, R. Nesper, J. Solid State Chem. 179 (2006) 1857–1863.
[26] A. Siedle, T. Wood, M. Brostrom, D. Koskenmaki, B. Montez, E. Oldfield, J. Am. Chem. Soc. 111 (1989) 1665–1669.
[27] K.R. Locherer, I.P. Swainson, E.K.H. Salje, J. Phys.: Condens. Matter 11 (1999) 4143–4156.